# Rapid condensation of the first Solar System solids

Yves Marrocchi, Johan Villeneuve, Emmanuel Jacquet, Maxime Piralla, Marc Chaussidon

# Rapid condensation of the first Solar System solids

Yves Marrocchi[a,1], Johan Villeneuve[a], Emmanuel Jacquet[b], Maxime Piralla[a], and Marc Chaussidon[c]

[a]Centre de Recherches Pétrographiques et Géochimiques (CRPG), CNRS, Université de Lorraine, UMR 7358, 54501 Vandoeuvre-lès-Nancy, France; [b]Institut de Minéralogie, de Physique des Matériaux et de Cosmochimie (IMPMC), CNRS & Muséum national d'Histoire naturelle, UMR 7590, 75005 Paris, France; and [c]Institut de Physique du Globe de Paris, Université de Paris, CNRS, 75238 Paris, France

Edited by Mark H. Thiemens, University of California San Diego, La Jolla, CA, and approved October 4, 2019 (received for review July 19, 2019)

**Chondritic meteorites are composed of primitive components formed during the evolution of the Solar protoplanetary disk. The oldest of these components formed by condensation, yet little is known about their formation mechanism because of secondary heating processes that erased their primordial signature. Amoeboid Olivine Aggregates (AOAs) have never been melted and underwent minimal thermal annealing, implying they might have retained the conditions under which they condensed. We performed a multiisotope (O, Si, Mg) characterization of AOAs to constrain the conditions under which they condensed and the information they bear on the structure and evolution of the Solar protoplanetary disk. High-precision silicon isotopic measurements of 7 AOAs from weakly metamorphosed carbonaceous chondrites show large, mass-dependent, light Si isotope enrichments ($-9‰ < \delta^{30}Si < -1‰$). Based on physical modeling of condensation within the protoplanetary disk, we attribute these isotopic compositions to the rapid condensation of AOAs over timescales of days to weeks. The same AOAs show slightly positive $\delta^{25}Mg$ that suggest that Mg isotopic homogenization occurred during thermal annealing without affecting Si isotopes. Such short condensation times for AOAs are inconsistent with disk transport timescales, indicating that AOAs, and likely other high-temperature condensates, formed during brief localized high-temperature events.**

meteorites | condensation | protoplanetary disk | isotopes

The proto-Sun and its surrounding protoplanetary disk formed 4.57 Ga ago from the gravitational collapse of the dense core of a molecular cloud. Chondrites are primitive meteorites left over from the evolution of the Solar protoplanetary disk. They comprise chondrules, fine-grained matrix, and the oldest known solids of the Solar System (1), refractory inclusions in the form of Ca- and Al-rich inclusions (CAIs, millimeter- to centimeter-sized high-temperature complex assemblages of refractory oxides and silicates; ref. 2) and amoeboid olivine aggregates (AOAs, fine-grained aggregates of olivine grains associated with variable proportions of CAI-like materials; ref. 3). The mineralogy of refractory inclusions resembles that of the earliest condensates predicted to form from a cooling gas of solar composition, with AOAs appearing to be somewhat lower-temperature objects than CAIs. This has long upheld the notion that the first solids of the Solar System formed by sequential gas–solid condensation of vaporized presolar matter (4–6), although many have undergone subsequent melting events, such as those which produced the ever-mysterious chondrules (e.g., ref. 7).

However, the timescales of condensation and/or partial evaporation during formation of AOAs and non-igneous CAIs remain largely underconstrained. Mere thermodynamics offer little insight into the "prehistory" of the solids and igneous cooling rates estimates refer to melting/crystallization events (8), not original gas–solid condensation. Al–Mg dating provides only an upper bound of a few 10s or 100s of millennia for the condensation epoch (9–12), which says little on the formation timescales of individual condensates. From an astrophysical viewpoint, evolution of isotherms should be fairly slow (on $10^4$ to $10^6$-y timescales; ref. 13) and random motions between significant condensation fronts should take similarly long (14), so it is often assumed that condensates formed over prolonged timescales (4, 15, 16). In contrast, Sugiura et al. (17) inferred from the absence of low-Ca pyroxene on most AOAs cooling rates >0.02 K/h at the end of olivine condensation and Komatsu et al. (18) derived 50 K/h from the presence of silica in one unusual AOA.

Stable isotopes may provide insights into the kinetics of gas–solid processes (19–21). Lighter isotopes are more gas-mobile and will thus preferentially impinge a solid grain, giving it an isotopically light composition provided that back-evaporation has not erased the initial fractionation. However, CAIs commonly show mass-dependent, heavy Si, Mg, O signatures (22) diagnostic of partial evaporation of refractory liquids resulting from the melting of solar condensates (23)—whose formation conditions are hereby blurred.

Yet the relatively fine-grained and sometimes porous AOAs have never been melted and have undergone only moderate thermal annealing during the evolution of the Solar protoplanetary disk (3, 24), implying they might represent fairly pristine condensates. Moreover, because AOAs record the condensation of olivine, which represented 1/3 of CI (Ivuna-like) chondritic matter (25)—second only to ice in terms of sheer mass—they are more representative of the protoplanetary disk than CAIs. However, in situ stable isotopic characterizations of AOAs have been performed only for oxygen, an element notoriously subject to poorly understood mass-independent fractionations within the protoplanetary disk, potentially blurring any mass-dependent condensation signal (26, 27). Here, we report the oxygen, silicon, and magnesium isotopic composition of Mg-rich olivine grains in AOAs from a set of carbonaceous chondrites characterized by minimal thermal metamorphism. We use our results to quantify the conditions under which primordial dust formed in the Solar System and discuss the

## Significance

Combined O, Si, Mg isotopic measurements of amoeboid olivine aggregates allow the individual condensation timescales of a typical set of the first Solar System solids to be estimated. Our results indicate formation over days or weeks, much faster than could be inferred from the secular evolution of the Solar protoplanetary disk. The oldest solids of the Solar System thus bear witness to a turbulent disk with strong thermal heterogeneities.

Author contributions: Y.M. and J.V. designed the study and performed the isotopic measurements; Y.M., J.V., E.J., M.P., and M.C. discussed the ion probe data; E.J. devised the astrophysical model; Y.M., J.V., E.J., and M.C. wrote the paper.

The authors declare no competing interest.

This article is a PNAS Direct Submission.



Data deposition: All raw SIMS data, summary of the data, and output of the model can be found at https://data.mendeley.com/datasets/dnxgdbzmzk/3.

[1]To whom correspondence may be addressed. Email: yvesm@crpg.cnrs-nancy.fr.

This article contains supporting information online at www.pnas.org/lookup/suppl/doi:10.1073/pnas.1912479116/-/DCSupplemental.

First published November 4, 2019.

implications on the structure and evolution of the Solar protoplanetary disk.

## Material and Methods

We surveyed all AOAs in a section each of Kaba (thin section N4075 from the Natural History Museum, Vienna, Austria), Northwest Africa (NWA) 5958 (thick section NWA 5958–1 from the Muséum national d'Histoire naturelle, Paris, France) and Miller Range (MIL) 07342 (thick section MIL 07342,9 from the NASA Antarctic Search for Meteorites program). Kaba is an oxidized Bali-like CV chondrite (28, 29). MIL 07342 is a CO chondrite. Although opaque assemblages are altered and evidence of incipient metasomatism appears on chondrule mesostasis, olivine compositions in type I chondrules (e.g., $Fo_{94.3–99.5}$) show no diffusional exchange; the chondrite is deemed of type 3.0–3.2 by the Antarctic Meteorite Petrographic Description database. NWA 5958 is a C2-ung CM-like chondrite, whose type II chondrule olivine Cr content as well as opaque petrography indicate minimal thermal metamorphism (<300 °C), yet chondrule mesostases have undergone extensive aqueous alteration, which did not affect olivine (30, 31).

Scanning electron microscope observations of AOAs were performed at CRPG-CNRS (Nancy, France) using a JEOL JSM-6510 with 3-nA primary beam at 15 kV. Quantitative compositional analyses of olivine in AOAs were performed using a CAMECA SX-100 electron microprobe [at CAMPARIS (Sorbonne Université, Paris, France)]. A 20-nA focused beam accelerated to 15-kV potential difference was used for spot analyses of olivine with 20-s analysis times. The PAP software was used for matrix corrections.

We analyzed the silicon isotopic compositions of olivines by secondary ion mass spectrometry (SIMS) using the multicollector CAMECA IMS 1270 E7 at CRPG. Olivines were sputtered with an ~5-nA primary $Cs^+$ beam set in Gaussian mode and accelerated at 10 kV (32). Secondary negative (28–30) $Si^-$ ions were accelerated at 10 kV and analyzed in multicollection mode on 3 off-axis Faraday cups (L′2, C, and H1, respectively). Charge accumulation on the sample surface was neutralized with an electron gun. The mass-resolving power was set at M/ΔM = 5,000 (slit 2) to completely resolve interferences on masses, refs. 28–30. The yields and backgrounds of the Faraday cups were calibrated at the beginning of each analytical session. Automatic centering of the transfer deflectors and mass was implemented in the analysis routine. A 10 × 10-$\mu m^2$ raster was applied to the primary beam to ensure flat-bottomed pits. We used 4 terrestrial standard materials (San Carlos olivine, synthetic forsterite, quartz, diopside) to define the terrestrial fractionation line. As there is no matrix effect for Si isotopes for olivine with Mg# (= 100 × Mg/[Mg+Fe]) above 70 (32), we used the San Carlos olivine to correct for instrumental mass fractionation. Measurements typically consisted of a 90-s presputtering, automatic mass and beam centering, and 50 cycles of 4-s integrations separated by 1-s waiting times. Thus, each measurement took ~7 min. Under these conditions, internal precision on $\delta^{29}Si$ and $\delta^{30}Si$ was ±0.05 through 0.30‰ and ±0.10 through 0.60‰ (2σ SE), respectively, depending on the sample, and the external reproducibility on $\delta^{29}Si$ and $\delta^{30}Si$ for the San Carlos olivine was ±0.10‰ and ±0.15‰, respectively (2σ SE). We also analyzed the oxygen and magnesium isotopic compositions of olivines in the same AOAs following previously established protocols (see *SI Appendix* for technical details).

## Results

AOAs in NWA 5958 and MIL 07342 have compact textures characterized by continuous olivine (Fig. 1 and *SI Appendix*, Figs. S1 and S2) (33). Ca–Al-rich vermicular patches are altered, although diopside persists, in AOAs in NWA 5958. AOAs in Kaba show smaller olivine zones, diopside, and Ca–Al-rich areas (*SI Appendix*, Fig. S3). Olivine in all AOAs investigated herein are Mg-rich with Mg# in the range 98.9 to 99.9 (*SI Appendix*, Table S1). AOA olivine grains have O isotopic compositions with $\delta^{18}O$ values ranging from −48.6 to −39.8‰, $\delta^{17}O$ values ranging from −47.7 to −41.5‰, and $\Delta^{17}O$ values ranging from −23.9 to −19.2‰ (*SI Appendix*, Fig. S4 and Table S2). The silicon isotopic compositions of AOA olivines show large, mass-dependent isotopic variations with $\delta^{29}Si$ values ranging from −5.1 to −1.0‰ and $\delta^{30}Si$ values ranging from −9.7 to −0.2‰ (Figs. 1 and 2 and *SI Appendix*, Table S3). We did not observe any correlation between the Si compositions and the analytical location within the AOAs (Fig. 1 and *SI Appendix*, Figs. S1 and S2). The magnesium isotopic compositions of olivines in AOAs show slightly positive $\delta^{25}Mg$ values ranging from 0.09 to 1.81‰ (Fig. 3 and *SI Appendix*, Table S4). We did not observe any correlation between the average Si and Mg isotopic compositions of the AOAs, nor with their elemental compositions.

**Duration and Contexts of AOA Condensation.** The mass-dependent character of the Si isotopic variations precludes their explanation by nucleosynthetic anomalies in the AOA-forming region. Provided bulk carbonaceous chondrites are a suitable proxy for the composition of the reservoir from which AOAs formed, the light isotope enrichment is also at variance with the positive 2‰/u fractionation expected from olivine-gas equilibrium (34) and inferred by ref. 15 to account for the Si isotopic variations of bulk chondrite. Partial evaporation would likewise produce heavy compositions in olivine, unless it occurred subordinately

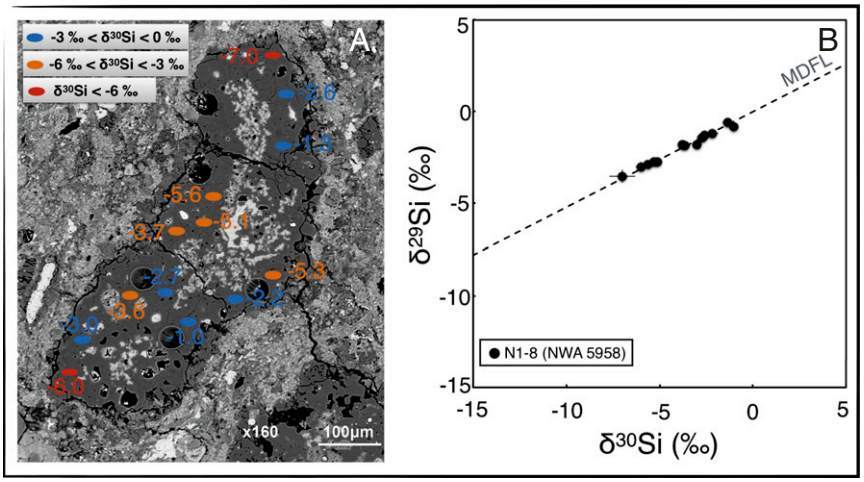


**Fig. 1.** A representative AOA and the Si isotopic compositions of its olivines. (*A*) Back-scattered electron image of AOA N1-8 from the CM-related chondrite NWA 5958 (30, 31). SIMS measurements are indicated by colored ellipses and the Si isotopic compositions associated with each analysis point. The color of the ellipses indicates the variability of the Si isotopic compositions by the range of the $\delta^{30}Si$ value: blue, −3‰ < $\delta^{30}Si$ < 0‰, orange, −6‰ < $\delta^{30}Si$ < −3‰, and red, $\delta^{30}Si$ < −6‰. (*B*) $\delta^{29}Si$ – $\delta^{30}Si$ diagram showing the mass-dependent variation observed in N1-8; MDFL, mass-dependent fractionation line.

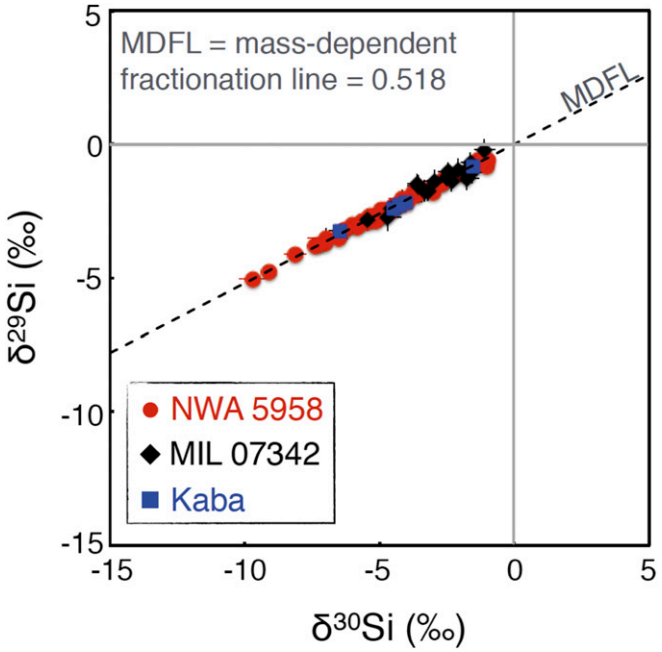


**Fig. 2.** Silicon 3-isotope plot showing the large range of mass-dependent isotopically light values measured in all analyzed AOAs in NWA 5958 (red), MIL 07342 (black), and Kaba (blue).

on isotopically lighter objects. In contrast, light isotopic enrichment would be expected from condensation, as the light isotopomers of gaseous SiO would collide with the growing solids at greater rates proportional to their thermal velocity (e.g., ref. 20)

$$v_{T,SiO} \equiv \sqrt{\frac{8kT}{\pi m_{SiO}}},$$

where $k$ is the Boltzmann constant, $T$ is the temperature, and $m_{SiO}$ is molecular mass. We note that the greatest observed Si isotopic fractionations, around −5‰/u (Fig. 2 and *SI Appendix*, Table S3), are not far from the maximum kinetic fractionations of −11‰/u, assuming that the condensation coefficient $\gamma_{SiO}$ has no mass dependence (*SI Appendix*, Fig. S5). This indicates back-evaporation has had little opportunity to curtail the isotopic fractionation of the condensate. This is possible if the reservoir temperature evolved through the olivine condensation interval over a time shorter than the "SiO condensation timescale," that is, the theoretical (e-folding) time of SiO condensation (on the available solids) in the absence of evaporation, given by (20) (*SI Appendix*):

$$t_{cond} \equiv \frac{1}{n_p \pi a^2 \gamma_{SiO} v_{T,SiO}},$$

where $n_p$ is the number density of condensate particles, assumed to be identical spheres of density $\rho_s = 3 \times 10^3$ kg/m$^3$ and radius $a$. If indeed the reservoir temperature evolved more rapidly than $t_{cond}$, high supersaturation would develop and make back-evaporation subdominant. In Fig. 4, we show the distribution of $\delta^{30}$Si expected for different cooling timescales $\lambda^{-1}$ ($\lambda$ being defined as the decay constant of the saturation density of Mg, related by stoichiometry to SiO; see *SI Appendix*). It is seen that only $\lambda t_{cond} > 1$, that is, $\lambda^{-1}$ values shorter than $t_{cond}$, can reproduce the range of the data. Thus, AOAs must have formed over a timescale of max($t_{cond}$, $\lambda^{-1}$)=$t_{cond}$.

So what is the magnitude of $t_{cond}$? For a steady $\alpha$ disk of mass accretion rate $\dot{M}$, using the pressure expression (*SI Appendix*), we have

$$t_{cond} = \frac{m_{SiO}^{1/2}}{32\gamma_{SiO} m_g^{5/6} T^{7/3}} \left(\frac{k\rho_s a \alpha \dot{M}}{\varepsilon_p}\right)^{1/3} \left(\frac{9\pi}{\sigma}\right)^{2/3}$$
$$= 10^5 \mathrm{s} \left(\frac{0.1}{\gamma_{SiO}}\right) \left(\frac{a}{30\mu\mathrm{m}}\right)^{1/3} \left(\frac{\alpha}{10^{-2}}\right)^{1/3} \left(\frac{\dot{M}}{10^{-7}\mathrm{M}_\odot/\mathrm{a}}\right)^{1/3}$$
$$\times \left(\frac{10^{-3}}{\varepsilon_p}\right)^{1/3} \left(\frac{1400\ \mathrm{K}}{T}\right)^{7/3},$$

where $\alpha$ is the turbulence parameter (35), $\sigma$ is the Stefan–Boltzmann constant, $m_g$ = 2.34 u is the mean nebular gas molecular mass, $\varepsilon_p$ is the solid/gas mass ratio, and $\mathrm{M}_\odot$ is the solar mass. Quite insensitively to the values of the disk parameters, our calculations thus reveal a short duration on the order of a day (~$10^5$ s) for the condensation of AOAs, or weeks if smaller values of $\gamma_{SiO}$ apply (e.g., ref. 36 and Fig. 4). This is consistent with the cooling rate lower limit of 0.02 K/h derived by (17) from the quasisystematic absence of low-Ca-pyroxene in AOAs, as well as the 50 K/h cooling rate suggested for the silica-bearing AOA of ref. 18. This may also account for the disequilibrium gas–solid condensation effects described for AOAs in Allan Hills 77037 (24).

Such durations are, however, much shorter than the $10^4$ to $10^6$-y timescales of secular evolution (and cooling) of the disk as a result of progressive accretion into the Sun (13). They are also much shorter than radial transport timescales, which ref. 37 estimated on the order of $10^3$ y (*SI Appendix*). Even vertical transport toward cooler surface layers, away from the disk midplane, would take much longer than the orbital period (38), even if winds are taken into account (*SI Appendix*). However, the smooth temperature profiles generally invoked in the inner disk are only average; heating would have been dictated by the dissipation of turbulence and likely prone to local heterogeneities, for instance in current sheets in magnetorotational instability-driven turbulence (39–41). Outside the "nominal" condensation front of forsterite, transient temperature excursions may have led to the olivine vaporization and recondensation. Perhaps late mixing with isotopically unfractionated SiO from the surroundings prevented the positive isotopic compositions predicted at the end of closed-system condensation (Fig. 4) but not observed in the data, although we cannot exclude an effect of the finite size of the ion probe beam (*SI Appendix*). In our model (illustrated schematically in Fig. 5), AOAs would have formed at

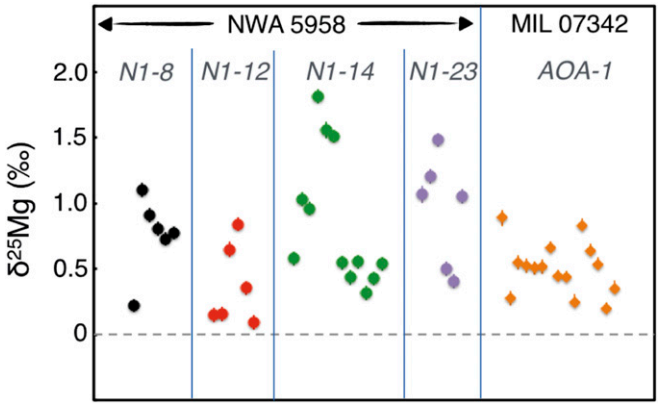


**Fig. 3.** $\delta^{25}$Mg values of AOAs analyzed in NWA 5958, MIL 07342, and Kaba.

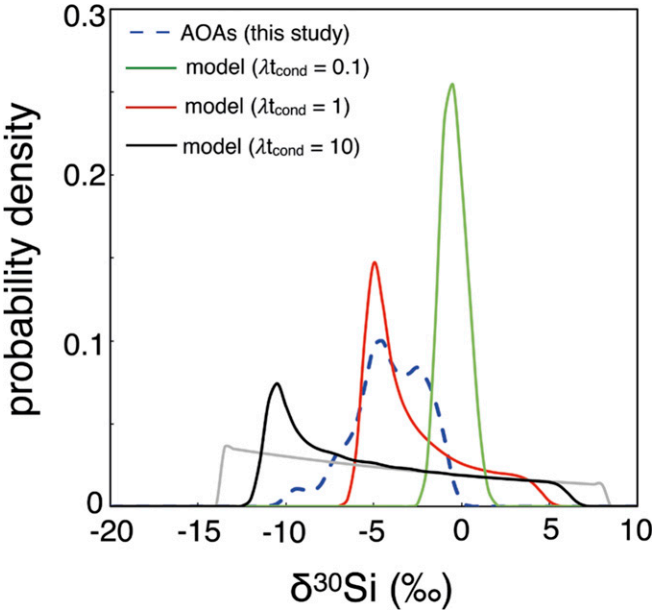


**Fig. 4.** Probability density of the $\delta^{30}$Si values of the studied AOAs (blue) compared to a closed-system condensation model. The model curves correspond to different speeds of evolution of the system, measured by the dimensionless parameter $\lambda t_{cond} = -t_{cond}\, d\ln n_{sat}/dt$ (where $n_{sat}$ is the saturation concentration of Mg; *SI Appendix*), with values of $\lambda t_{cond}$ = 0.1 (green), 1 (blue), 10 (black), and ∞ (gray). The range of Si isotopic fractionations observed herein can only be reproduced when $\lambda t_{cond} > 1$, although different thermal histories are likely convolved in the measured distribution.

greater heliocentric distances than a mere consideration of the average isotherms would suggest. Those which we now see in chondrites would have eventually escaped the evaporation/recondensation cycle of their matter during outward migration toward less-heated regions, e.g., as a result of turbulent diffusion or disk expansion (13, 42, 43). The "frozen-in" AOAs would then have eventually reached the cold regions of chondrite accretion.

Similar processes would likely hold for higher-temperature condensates, i.e., CAIs, at shorter heliocentric distances. There may thus be a continuum between the condensation processes and subsequent reheating events that led to their remelting and crystallization, with cooling rates on the of order 0.1 to 10 K/h (8)—not to mention chondrule-forming processes as well, with cooling rates estimates spanning 1 to 3,000 K/h (ref. 44 and references therein)—the formation of Wark–Lovering rims (45–47) and/or partial evaporation resulting in heavy isotopic enrichments (19). The isolation of the ultrarefractory component presumably lost from the parent reservoir of numerous group II CAIs (48) may have likewise required similarly short timescales. Indeed, the light isotopic enrichment of (refractory) heavy rare-earth elements in such CAIs (49) allows for only limited recondensation during the partial evaporation of the now-lost ultrarefractory complement.

**Condensate Agglomeration.** It is instructive to compare the condensation timescale calculated above to the grain–grain collision timescale $t_{coll}$—that is, the mean time between 2 collisions for a given grain, given by ref. 50:

$$t_{coll} \equiv \frac{1}{n_p 4\pi a^2 \Delta v_{coll}},$$

where $\Delta v_{coll}$ is the typical particle–particle velocity. Comparing the 2 timescales, we obtain

$$\frac{t_{coll}}{t_{cond}} = \frac{\gamma_{SiO} v_{T,SiO}}{4\Delta v_{coll}} = 20\left(\frac{\gamma_{SiO}}{0.1}\right)\left(\frac{1\ \mathrm{m/s}}{\Delta v_{coll}}\right)\left(\frac{T}{1{,}400\ \mathrm{K}}\right)^{1/2}.$$

Since $\Delta v_{coll}$ is normalized to an upper bound (the critical fragmentation or bouncing velocity; ref. 51), $t_{coll}$ is resolvably longer than $t_{cond}$, implying that aggregation of individual condensates, if colliding below the critical velocity for agglomeration [which might have been greater for higher temperatures (52)], generally occurred after, not during, condensation (Fig. 5). Indeed, unmelted fine-grained CAIs are composed of mineralogically zoned sub–100-μm nodules with more refractory minerals concentrated in their center, consistent with an origin as individual condensates, which encompassed the whole refractory condensation sequence before coagulation (53). Still, because $t_{coll}$ should be much shorter than radial or vertical transport timescales (14), agglomeration should have occurred largely between genetically related bodies. This accounts for the generally fairly uniform character of fine-grained CAIs at mesoscale, notwithstanding common macroscale layering (53, 54). Same holds for AOAs. One can envision that the high-temperature events that ultimately led to their final condensation likely first evaporated all but the most refractory (CAI-like) phases of any dust grains present. Olivine recondensation would have then mantled these dust grains; perhaps some olivine also condensed homogeneously (such as the $^{16}$O-rich ones found in chondrite matrices, refs. 55 and 56). These different olivine-bearing bodies would have then aggregated together. While, as argued above, aggregated bodies might have genetic relationships to one another, they may represent different thermal events, if $t_{coll}$ was longer than transport timescales or evaporation/recondensation cycles, and thus possibly variable thermal histories. Thus, individual AOAs may group bodies with similar or various ranges in Si isotopic fractionation. Depending on the recondensation events sampled by individual AOAs, different AOAs may vary in their ranges of $\delta^{30}$Si.

**Secondary Heating of Amoeboid Olivine Aggregates.** Since $\delta^{25}$Mg corresponds to similar isotopomer mass ratios as $\delta^{30}$Si (in terms of Mg and SiO, respectively), one would expect similar fractionations for the former in AOAs (*SI Appendix*). Mg isotope fractionations as large as –14‰/u have been reported in fine-grained CAIs in Allende (57, 58). However, we observe little variation of $\delta^{25}$Mg in the AOAs analyzed herein (only 0.4‰ SD), although (59) reported $\delta^{25}$Mg down to –3‰ in some porous AOAs in Kaba. The compact textures of our AOAs suggest significant postagglomeration annealing, which may have led to the Mg isotopic homogenization given the much higher diffusivity of Mg relative to Si (60). Indeed, for a Mg diffusion coefficient of ~$10^{-17}$ $m^2/s$ at 1,400 K, isotopic homogenization over lengths of 50 μm requires only an integrated (possibly discontinuous) time of a decade or so (Fig. 5), whereas O and Si homogenization requires durations of 6 orders of magnitude longer. A timescale of a decade would agree with 1) the <60 y of isotopic exchange with $^{16}$O-poor gas for 2 Leoville AOAs (61) and 2) the effective cooling rate of 0.002 K/h estimated from the closure of Mn and Cr diffusion in AOA olivine (17). Ca from the Ca–Al-rich nodules would have diffused as well into forsterite (17, 31), accounting for its apparent Ca enrichment in compact AOAs (3, 17, 31), which our Si isotopic results no longer allow to explain by a condensation slower than for porous AOAs (17).

The closure of the Mg isotopic system in AOAs would postdate the condensation and aggregation period but would not have been as late as parent body metamorphism, because AOAs retain near-canonical Al–Mg mineral isochrons (e.g., refs. 62 and 63). The Mg isotopic composition of the bulk olivine (to which all olivines would have been homogenized) would have been also closer to the reservoir average than that of Si because Mg would be essentially completely condensed during olivine condensation,

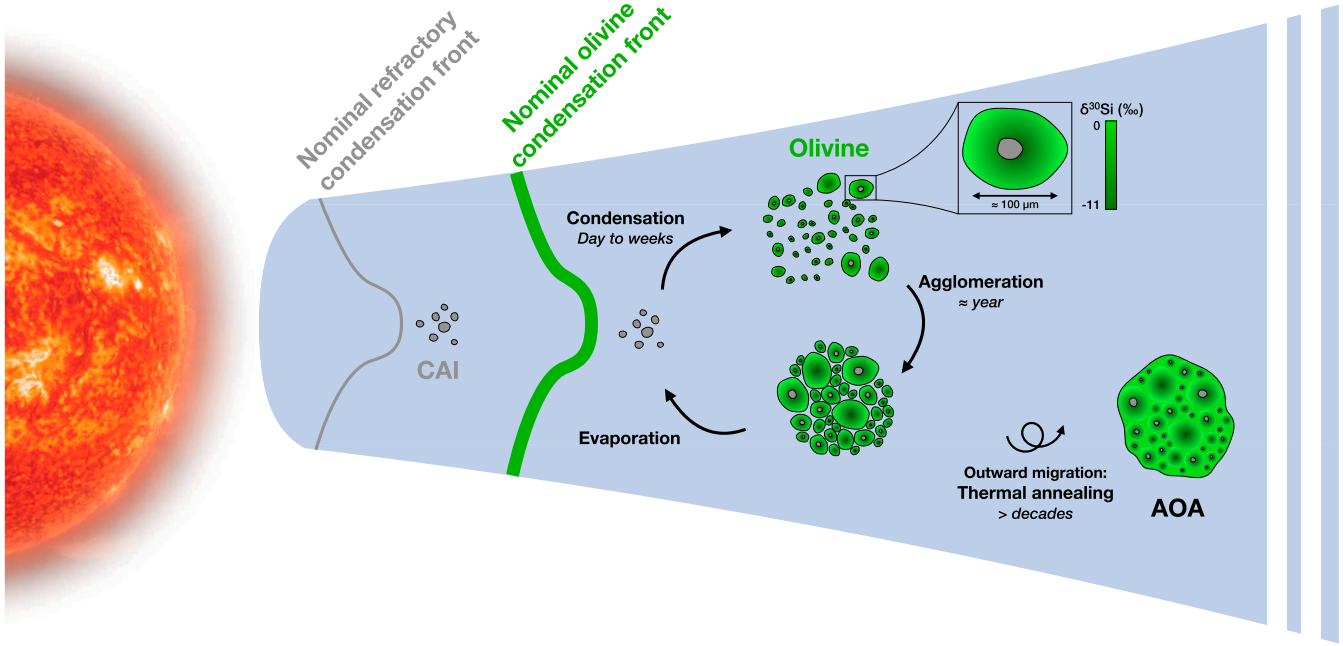


**Fig. 5.** Schematic representation of AOA formation. Localized heating beyond the nominal olivine condensation front may have evaporated solids, leaving refractory residues. Upon cooling, such CAI-like materials served as seeds for olivine condensation slightly beyond the nominal olivine condensation front. The rapid condensation inferred herein (day to weeks) would have produced large negative mass-dependent silicon isotopic fractionations. Agglomeration of AOAs occurred over a longer timescale on the order of a year. Subsequent thermal annealing produced the AOAs as we observe them today, homogenizing their Mg isotopic compositions without affecting their silicon isotopic compositions.

while almost half of the original SiO would still remain (ref. 6 and *SI Appendix*).

In conclusion, our results suggest that the earliest solids of the Solar System condensed, aggregated, and were processed over short timescales, perhaps on the order of days, in a dynamic and thermally nonuniform disk. Nowhere was the primordial condensation sequence quiescent.

**Data Availability.** All of the data are available in the *SI Appendix* (*SI Appendix*, Tables S1–S4). All raw SIMS data, summary of the data, and output of the model can be accessed here: https://data.mendeley.com/datasets/dnxgdbzmzk/3.

**ACKNOWLEDGMENTS.** The authors are grateful to Nordine Bouden for his assistance with isotopic measurements. We thank the Muséum national d'Histoire naturelle (Paris, France), the Natural History Museum of Vienna (Austria), and the Antarctic Search for Meteorites (ANSMET) program for loaning the NWA 5958, Kaba, and MIL 07342 sections. US Antarctic meteorite samples are recovered by ANSMET, funded by NSF and NASA, and characterized and curated by the Department of Mineral Sciences of the Smithsonian Institution and Astromaterials Curation Office at NASA Johnson Space Center. This research was funded by l'Agence Nationale de la Recherche (ANR) through Grant ANR-14-CE33-0002-01 SAPINS (Principal Investigator [PI] Y.M.), ANR-18-CE31-0010-01 CASSYSS (PI J.V.), and ANR-15-CE31-0004-1 CRADLE (PI M.C.). Tim Fagan and an anonymous reviewer are thanked for constructive comments. This is CRPG-CNRS Contribution 2715.

1. Y. Amelin *et al.*, U–Pb chronology of the Solar System's oldest solids with variable $^{238}U/^{235}U$. *Earth Planet. Sci. Lett.* **300**, 343–350 (2010).
2. G. J. MacPherson, "Calcium–aluminum-rich inclusions in chondritic meteorites" in *Meteorites and Cosmochemical Processes*, A. M. Davis, Ed. (Elsevier, 2014), pp. 139–179.
3. A. N. Krot *et al.*, Amoeboid olivine aggregates and related objects in carbonaceous chondrites: Records of nebular and asteroid processes. *Geochemistry* **64**, 185–239 (2004)
4. J. Larimer, Chemical fractionations in meteorites—I. Condensation of the elements. *Geochim. Cosmochim. Acta* **31**, 1215–1238 (1967).
5. L. Grossman, Condensation in the primitive solar nebula. *Geochim. Cosmochim. Acta* **36**, 597–619 (1972).
6. A. M. Davis, F. Richter, "Condensation and evaporation of solar system materials" in *Meteorites and Cosmochemical Processes*, A. M. Davis, Ed. (Elsevier, 2014), pp. 335–360.
7. Y. Marrocchi *et al.*, Formation of CV chondrules by recycling of amoeboid olivine aggregate-like precursors. *Geochim. Cosmochim. Acta* **247**, 121–141 (2019).
8. E. Stolper, J. M. Paque, Crystallization sequences of Ca-Al-rich inclusions from Allende: The effects of cooling rate and maximum temperature. *Geochim. Cosmochim. Acta* **50**, 1785–1806 (1986).
9. G. J. MacPherson, N. T. Kita, T. Ushikubo, E. S. Bullock, A. M. Davis, Well-resolved variations in the formation ages for Ca–Al-rich inclusions in the early Solar System. *Earth Planet. Sci. Lett.* **331-332**, 43–54 (2012).
10. K. K. Larsen *et al.*, Evidence for magnesium isotope heterogeneity in the solar protoplanetary disk. *Astrophys. J.* **735**, L37 (2011).
11. K. Thrane, M. Bizzarro, J. A. Baker, Extremely brief formation interval for refractory inclusions and uniform distribution of $^{26}Al$ in the early solar system. *Astrophys. J.* **646**, L159–L162 (2006).
12. R. K. Mishra, M. Chaussidon, Timing and extent of Mg and Al isotopic homogenization in the early inner Solar System. *Earth Planet. Sci. Lett.* **390**, 318–326 (2014).
13. F. C. Pignatale, S. Charnoz, M. Chaussidon, E. Jacquet, Making the planetary material diversity during the early assembling of the solar system. *Astrophys. J.* **867**, L23–L27 (2018).
14. S. Charnoz, J. Aléon, N. Chaumard, K. Baillié, E. Taillifet, Growth of calcium–aluminum-rich inclusions by coagulation and fragmentation in a turbulent protoplanetary disk: Observations and simulations. *Icarus* **252**, 440–453 (2015).
15. N. Dauphas, F. Poitrasson, C. Burkhardt, H. Kobayashi, K. Kurosawa, Planetary and meteoritic Mg/Si and $\delta^{30}Si$ variations inherited from solar nebula chemistry. *Earth Planet. Sci. Lett.* **427**, 236–248 (2015).
16. L. Grossman, Vapor-condensed phase processes in the early solar system. *Meteorit. Planet. Sci.* **45**, 7–20 (2010).
17. N. Sugiura, M. I. Petaev, A. Miyazaki, H. Hyagon, Nebular history of amoeboid olivine aggregates. *Meteorit. Planet. Sci.* **44**, 559–572 (2009).
18. M. Komatsu *et al.*, First evidence for silica condensation within the solar protoplanetary disk. *Proc. Natl. Acad. Sci. U.S.A.* **115**, 7497–7502 (2018).
19. F. M. Richter, A. M. Davis, D. S. Ebel, A. Hashimoto, Elemental and isotopic fractionation of type B calcium-, aluminum-rich inclusions: Experiments, theoretical considerations, and constraints on their thermal evolution. *Geochim. Cosmochim. Acta* **66**, 521–540 (2002).
20. F. M. Richter, Timescales determining the degree of kinetic isotope fractionation by evaporation and condensation. *Geochim. Cosmochim. Acta* **68**, 4971–4992 (2004).
21. F. M. Richter, P. E. Janney, R. A. Mendybaev, A. M. Davis, M. Wadhwa, Elemental and isotopic fractionation of Type B CAI-like liquids by evaporation. *Geochim. Cosmochim. Acta* **71**, 5544–5564 (2007).

22. R. N. Clayton, R. W. Hinton, A. M. Davis, Isotopic variations in the rock-forming elements in meteorites. *Philos. Trans. R. Soc. A Math. Phys. Eng. Sci.* **325**, 483–501 (1988).
23. L. Grossman *et al*., Primordial compositions of refractory inclusions. *Geochim. Cosmochim. Acta* **72**, 3001–3021 (2008).
24. J. Han, A. J. Brearley, Microstructural evidence for complex formation histories of amoeboid olivine aggregates from the ALHA77307 CO3.0 chondrite. *Meteorit. Planet. Sci.* **50**, 904–925 (2015).
25. S. Yoneda, L. Grossman, Condensation of CaO-MgO-$Al_2O_3$-$SiO_2$ liquids from cosmic gases. *Geochim. Cosmochim. Acta* **59**, 3413–3444 (1995).
26. L. Kööp *et al*., A link between oxygen, calcium and titanium isotopes in $^{26}$Al-depleted hibonite-rich CAIs from Murchison and implications for the heterogeneity of dust reservoirs in the solar nebula. *Geochim. Cosmochim. Acta* **189**, 70–95 (2016).
27. J. Aléon, Closed system oxygen isotope redistribution in igneous CAIs upon spinel dissolution. *Earth Planet. Sci. Lett.* **482**, 324–333 (2018).
28. H. Y. McSween, Petrographic variations among carbonaceous chondrites of the Vigarano type. *Geochim. Cosmochim. Acta* **41**, 1777–1790 (1977).
29. Y. Marrocchi, M. Chaussidon, L. Piani, G. Libourel, Early scattering of the solar protoplanetary disk recorded in meteoritic chondrules. *Sci. Adv.* **2**, e1601001 (2016).
30. E. Jacquet *et al*., Northwest Africa 5958: A weakly altered CM-related ungrouped chondrite, not a CI3. *Meteorit. Planet. Sci.* **51**, 851–869 (2016).
31. E. Jacquet, Y. Marrocchi, Chondrule heritage and thermal histories from trace element and oxygen isotope analyses of chondrules and amoeboid olivine aggregates. *Meteorit. Planet. Sci.* **52**, 2672–2694 (2017).
32. J. Villeneuve, M. Chaussidon, Y. Marrocchi, Z. Deng, E. B. Watson, High-precision in situ silicon isotopic analyses by multi-collector secondary ion mass spectrometry in olivine and low-calcium pyroxene. *Rapid Commun. Mass Spectrom.* **33**, 1589–1597 (2019).
33. Y. Marrocchi, Data from "AOAs - Marrocchi." Mendeley Data. http://dx.doi.org/10.17632/dnxgdbzmzk.3. Accessed 7 October 2019.
34. M. Javoy, E. Balan, M. Méheut, M. Blanchard, M. Lazzeri, First-principles investigation of equilibrium isotopic fractionation of O- and Si-isotopes between refractory solids and gases in the solar nebula. *Earth Planet. Sci. Lett.* **319-320**, 118–127 (2012).
35. N. I. Shakura, R. A. Sunyaev, "Black holes in binary systems: Observational appearances" in *X- and Gamma-Ray Astronomy. International Astronomical Union/Union Astronomique Internationale*, H. Bradt, R. Giacconi, Eds. (Springer, Dordrecht, 1973), vol. 55, pp. 155–164.
36. S. Tachibana, A. Takigawa, A. Miyake, H. Nagahara, K. Ozawa, "Condensation of forsterite under controlled protoplanetary disk conditions" in *45$^{th}$ Lunar and Planetary Science Conference* (The Woodlands, Lunar and Planetary Institute, Houston, TX, 2014), ID 1226.
37. E. Taillifet, K. Baillié, S. Charnoz, J. Aléon, "Insights on CAIs thermal history from turbulent transport simulations of micron-sized precursors in the Early Solar Nebula" in *44$^{th}$ Lunar and Planetary Science Conference* (2013).
38. F. J. Ciesla, Residence times of particles in diffusive protoplanetary disk environments. I. vertical motions. *Astrophys. J.* **723**, 514–529 (2010).
39. S. Hirose, N. J. Turner, Heating and cooling protostellar disks. *Astrophys. J.* **732**, L30–L35 (2011).
40. M. Flock, S. Fromang, M. González, B. Commerçon, Radiation magnetohydrodynamics in global simulations of protoplanetary discs. *A&A* **560**, A43–A14 (2013).
41. C. P. McNally, A. Hubbard, C.-C. Yang, M. M. Mac Low, Temperature fluctuations driven by magnetorotational instability in protoplanetary disks. *Astrophys. J.* **791**, 62–77 (2014).
42. J. N. Cuzzi, S. S. Davis, A. R. Dobrovolski, Blowing in the wind. II. Creation and redistribution of refractory inclusions in a turbulent protoplanetary nebula. *Icarus* **166**, 385–402 (2003).
43. L. Yang, F. J. Ciesla, The effects of disk building on the distributions of refractory materials in the solar nebula. *Meteorit. Planet. Sci.* **47**, 99–119 (2015).
44. R. H. Jones, J. Villeneuve, G. Libourel, "Thermal histories of chondrules" in *Chondrules: Records of Protoplanetary Disk Processes*, S. S. Russell, H. C. Connolly, A. N. Krot, Eds. (Cambridge University Press, 2018), pp 57–90.
45. D. A. Wark, J. F. Lovering, "Marker events in the early evolution of the solar system-Evidence from rims on Ca-Al-rich inclusions in carbonaceous chondrites" in *Lunar Science Conference, 8th* (Pergamon Press, New York, NY, 1977), vol. 1, pp. 95–112.
46. J.-D. Bodénan, N. A. Starkey, S. S. Russell, I. P. Wright, I. A. Franchi, An oxygen isotope study of Wark–Lovering rims on type A CAIs in primitive carbonaceous chondrites. *Earth Planet. Sci. Lett.* **401**, 327–336 (2014).
47. J. L. Simon *et al*., Oxygen isotopic variations in the outer margins and Wark-Lovering rims of refractory inclusions. *Geochim. Cosmochim. Acta* **186**, 242–276 (2016).
48. B. Mason, S. R. Taylor, Inclusions in the Allende meteorite. *Smithson. Contrib. Earth Sci.* **25**, 1–33 (1982).
49. J. Y. Hu, N. Dauphas, F. L. H. Tissot, R. Yokochi, T. J. Ireland, "Insights into Evaporation/Condensation Processes in the Early Solar System from Mass-Dependent Fractionations of REEs in Type II CAIs" in *50$^{th}$ Lunar and Planetary Science Conference* (The Woodlands, Lunar and Planetary Institute, Houston, TX, 2019), ID 1938.
50. Y. Nakagawa, K. Nakazawa, C. Hayashi, Growth and sedimentation of dust grains in the primordial solar nebula. *Icarus* **45**, 517–528 (1981).
51. E. Jacquet, The quasi-universality of chondrule size as a constraint for chondrule formation models. *Icarus* **232**, 176–186 (2014).
52. A. Hubbard, Making terrestrial planets: High temperatures, FU orionis outbursts, earth, and planetary system Architectures. *Astrophys. J.* **840**, L5–L6 (2017).
53. A. N. Krot, G. J. MacPherson, A. A. Ulyanov, M. I. Petaev, Fine-grained, spinel-rich inclusions from the reduced CV chondrites Efremovka and Leoville: I. Mineralogy, petrology, and bulk chemistry. *Meteorit. Planet. Sci.* **39**, 1517–1553 (2004).
54. J. Aléon, A. N. Krot, K. D. McKeegan, Calcium-aluminum-rich inclusions and amoeboid olivine aggregates from the CR carbonaceous chondrites. *Meteorit. Planet. Sci.* **37**, 1729–1755 (2002).
55. T. Kunihiro, K. Nagashima, H. Yurimoto, Microscopic oxygen isotopic homogeneity/heterogeneity in the matrix of the Vigarano CV3 chondrite. *Geochim. Cosmochim. Acta* **69**, 763–773 (2005).
56. M. Cosarinsky, L. A. Leshin, G. J. MacPherson, Y. Guan, A. N. Krot, Chemical and oxygen isotopic compositions of accretionary rim and matrix olivine in CV chondrites: Constraints on the evolution of nebular dust. *Geochim. Cosmochim. Acta* **72**, 1887–1913 (2008).
57. C. A. Brigham, D. Papanastassiou, G. J. Wasserburg, "Mg isotopic heterogeneities in fine-grained Ca-Al inclusions" in *16$^{th}$ Lunar and Planetary Science Conference* (Lunar and Planetary Institute, Houston, TX, 1985).
58. C. A. Brigham, I. D. Hutcheon, D. Papanastassiou, G. J. Wasserburg, "Evidence for $^{26}$Al and Mg isotopic heterogeneity in a fine-grained CAI" in *17$^{th}$ Lunar and Planetary Science Conference* (Lunar and Planetary Institute, Houston, TX, 1986).
59. K. Fukuda *et al*., "The relationship between oxygen and magnesium isotope ratios in olivine from the comet 81P/Wild 2: A comparison with AOAs in primitive meteorites" in *50$^{th}$ Lunar and Planetary Science Conference* (The Woodlands, Lunar and Planetary Institute, Houston, TX, 2019), ID 1989.
60. S. Chakraborty, Diffusion coefficients in Olivine, Wadsleyite and Ringwoodite. *Rev. Mineral. Geochem.* **72**, 603–639 (2010).
61. T. J. Fagan, A. N. Krot, K. Keil, H. Yurimoto, Oxygen isotopic evolution of amoeboid olivine aggregates in the reduced CV3 chondrites Efremovka, Vigarano, and Leoville. *Geochim. Cosmochim. Acta* **68**, 2591–2611 (2004).
62. S. Itoh, A. E. Rubin, H. Kojima, J. T. Wasson, H. Yurimoto, "Amoeboid olivine aggregates and AOA-bearing chondrule from Y-81020 CO3.0 chondrite: Distribution of oxygen and magnesium isotopes." in *33$^{rd}$ Annual Lunar and Planetary Science Conference* (Lunar and Planetary Institute, Houston, TX, 2002), ID 1490.
63. A. N. Krot, C. Park, K. Nagashima, Amoeboid olivine aggregates from CH carbonaceous chondrites. *Geochim. Cosmochim. Acta* **139**, 131–153 (2014).